UNIVERSITY OF BIRMINGHAM
University of Birmingham Research at Birmingham

Characterisation of the multiphase fluid dynamics of the CoarseAIR™ fluidised bed flotation cell using the Large Modular Array (LaMA) for positron emission particle tracking (PEPT)

Mesa, Diego; Hampel, Dawid M.; Neethling, Stephen J.; Kokalova Wheldon, Tzany; Brito-Parada, Pablo R.

DOI:
10.1016/j.mineng.2024.108700

License:
Creative Commons: Attribution (CC BY)

Document Version
Publisher's PDF, also known as Version of record

Citation for published version (Harvard):
Mesa, D, Hampel, DM, Neethling, SJ, Kokalova Wheldon, T & Brito-Parada, PR 2024, 'Characterisation of the multiphase fluid dynamics of the CoarseAIR™ fluidised bed flotation cell using the Large Modular Array (LaMA) for positron emission particle tracking (PEPT)', *Minerals Engineering*, vol. 211, 108700. https://doi.org/10.1016/j.mineng.2024.108700

Link to publication on Research at Birmingham portal

General rights
Unless a licence is specified above, all rights (including copyright and moral rights) in this document are retained by the authors and/or the copyright holders. The express permission of the copyright holder must be obtained for any use of this material other than for purposes permitted by law.

•Users may freely distribute the URL that is used to identify this publication.
•Users may download and/or print one copy of the publication from the University of Birmingham research portal for the purpose of private study or non-commercial research.
•User may use extracts from the document in line with the concept of 'fair dealing' under the Copyright, Designs and Patents Act 1988 (?)
•Users may not further distribute the material nor use it for the purposes of commercial gain.

Where a licence is displayed above, please note the terms and conditions of the licence govern your use of this document.

When citing, please reference the published version.

Take down policy
While the University of Birmingham exercises care and attention in making items available there are rare occasions when an item has been uploaded in error or has been deemed to be commercially or otherwise sensitive.

If you believe that this is the case for this document, please contact UBIRA@lists.bham.ac.uk providing details and we will remove access to the work immediately and investigate.

Download date: 04. May. 2024

Minerals Engineering 211 (2024) 108700

Contents lists available at ScienceDirect

Minerals Engineering

journal homepage: www.elsevier.com/locate/mineng

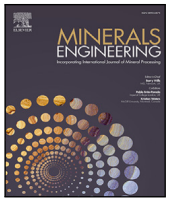

Characterisation of the multiphase fluid dynamics of the CoarseAIR™ fluidised bed flotation cell using the Large Modular Array (LaMA) for positron emission particle tracking (PEPT)

Diego Mesa [a,*], Dawid M. Hampel [b], Stephen J. Neethling [a], Tzany Kokalova Wheldon [b], Pablo R. Brito-Parada [a]

[a] Advanced Mineral Processing Research Group, Royal School of Mines, Imperial College London, United Kingdom
[b] Positron Imaging Centre, School of Physics and Astronomy, University of Birmingham, United Kingdom

ARTICLE INFO

Keywords:
CoarseAIR™ flotation cell
Positron emission particle tracking (PEPT)
Large Modular Array (LaMA)
Multiphase fluid dynamics
Fluidised bed flotation cell

ABSTRACT

Fluidised bed flotation cells (FBFCs) present a compelling solution for coarse particle flotation, enabling an increase in the target particle size in comminution circuits, with the corresponding energy savings. Despite their potential and strong industrial interest, the three-phase fluid dynamics of large-scale FBFCs remain unexplored due to measurement complexities and size restrictions. This paper presents the first quantification of the fluid dynamics of the CoarseAir™-100, a 2 m tall laboratory-scale FBFC. Measurements were obtained using positron emission particle tracking (PEPT), a non-invasive technique that tracks the motion of a radiolabelled tracer. Leveraging the Large Modular Array (LaMA) PEPT system, consisting of 48 buckets, each housing four detector blocks, this study is the largest PEPT experiment to date. Particle tracks of hydrophobic and hydrophilic tracers were obtained under different fluidisation and airflow rates. Hydrophobic tracers exhibited buoyant behaviour despite their large size of up to 700 μm, while hydrophilic tracers engaged in recirculation patterns with rapid downward motion near the walls. The intricate motion of particles in the lamella plates was experimentally quantified, revealing an average path tortuosity of 7.3, providing essential information for design. These results represent a major advance in our understanding of fluidised bed flotation cells, contributing to the refinement of design and scale-up strategies for FBFCs.

1. Introduction

Froth flotation is the most important and widely used technique in the mineral processing industry, being a key step in the production of critical raw materials. The flotation process requires the particles to be reduced in size in order to partially liberate the surface of the valuable minerals for bubble-particle attachment. However, the grinding process is highly inefficient (Hassanzadeh, 2018; Hassanzadeh et al., 2022), using up to 70% of the total energy consumption of a typical mining operation (Deniz, 2013; Hassanzadeh, 2018). It has been reported that approximately 3% of the world's electricity is consumed in mineral comminution (Deniz, 2013; Chelgani et al., 2019; Kromah et al., 2022). Consequently, significant efforts have been directed towards the flotation of coarse particles in order to reduce grinding requirements.

Coarse material in froth flotation is usually defined as particles with a diameter greater than 250 μm. The flotation of coarse material is challenging due to the high probability of detachment of particles from the surface of the bubbles (Wang et al., 2016; Hassanzadeh et al., 2022), which is enhanced by the turbulent regime of conventional flotation cells. Moreover, even if coarse particles remain attached to the bubbles, the low buoyancy of the particle-bubble aggregates hinders coarse flotation efficiency (Jameson, 2010; Kromah et al., 2022; Hassanzadeh et al., 2022).

Several new designs of flotation equipment have been proposed to tackle these two specific challenges of coarse flotation (Hassanzadeh et al., 2022). Among them, the most promising designs consist of fluidised bed flotation cells, including Eriez's HydroFloat™ (Kohmuench et al., 2001; Fosu et al., 2015; Islam and Nguyen, 2020; Zanin et al., 2021), Jord's NovaCell™ (Jameson and Emer, 2019; Jameson et al., 2020), and most recently FLSmidth's CoarseAIR™ (Crompton et al., 2022). Two comprehensive reviews of fluidised bed flotation cells for coarse flotation can be found in Kromah et al. (2022) and Janishar Anzoom et al. (2024).

Fluidised bed flotation cells operate under the principle of hindered settling, which involves the suspension of particles in a teeter bed (Wills

* Corresponding author.
E-mail addresses: d.mesa@imperial.ac.uk (D. Mesa), d.hampel@pgr.bham.ac.uk (D.M. Hampel).

https://doi.org/10.1016/j.mineng.2024.108700
Received 31 January 2024; Received in revised form 4 April 2024; Accepted 9 April 2024
Available online 19 April 2024
0892-6875/© 2024 The Author(s). Published by Elsevier Ltd. This is an open access article under the CC BY license (http://creativecommons.org/licenses/by/4.0/).

and Finch, 2016; Kromah et al., 2022). The upward flow of water generates a fluidised bed of suspended particles. The injected air bubbles attach to the exposed hydrophobic surface of the coarse particles, forming bubble-particle aggregates with low apparent density. These aggregates still lack the required buoyancy to ascend independently, as highlighted for conventional flotation cells. However, in fluidised bed flotation, these aggregates can rise to the top of the teeter bed because of their lower density and ultimately overflow from the cell.

To prevent the detachment of coarse particles, fluidised bed flotation cells need to have quiescent regimes, avoiding zones of turbulent mixing. Although there are several publications of Computational Fluid Dynamics (CFD) simulations for different fluidised bed flotation cells (Hamidipour et al., 2012; Dickinson and Galvin, 2014; Galvin and Dickinson, 2014; Galvin et al., 2014; Islam and Nguyen, 2020), there is a distinct lack of experimental fluid dynamics data associated with this type of equipment. Han et al. (2022) conducted an experiment in a three-phase fluidised bed flotation column, where the solid phase was represented by steel balls. However, their results obtained with image analysis are limited to general observations such as bed fluctuation ratio, gas holdup and bubble size distribution, and do not explore the dynamics of the fluids and particles involved.

This gap in the literature is not an isolated issue for three-phase fluidised bed flotation cells. The experimental characterisation of flotation multiphase fluid dynamics is a challenging problem, which has only recently been tackled using positron emission particle tracking (PEPT).

1.1. Positron emission particle tracking (PEPT)

Positron emission particle tracking, or PEPT, is a non-invasive technique utilised to monitor the position of a tracer particle over time (Parker et al., 1993). This technique uses penetrating radiation and is not dependent on optical properties, making it suitable for tracking a particle within opaque and dense systems such as a flotation cell. This is a key advantage over other experimental techniques, such as Particle Image Velocimetry (PIV), which are typically limited to single or dilute two-phase systems, as they are based on optical properties.

In PEPT experiments, a tracer particle radiolabelled with a short-lived, positron-emitting isotope is tracked using a positron-sensitive detector array such as a positron emission tomography (PET) camera. The positron emitted by the tracer annihilates with an electron from local matter, producing a pair of 511 keV almost back-to-back γ-rays. If the PET camera detects both γ-rays from the pair in coincidence within a set coincidence time window, the annihilation event can be located somewhere along the path between the two detectors, forming a line of response (LOR). With multiple LORs, the location of a moving tracer particle can be triangulated with time, providing time series data on the tracer's location, which can be used to determine the tracer velocity.

In the last decade, PEPT has been increasingly used to evaluate the fluid dynamics of complex multiphase mineral processing applications, including froth flotation (Mesa et al., 2021, 2022; Cole et al., 2022b,a). Although there have been many developments on its use and capabilities, PEPT is still a novel and specialised technique, available in a handful of laboratories worldwide, due to the need for a cyclotron to produce radioactive material. Another limitation for its widespread use has been the maximum size of equipment that can be positioned within a PET camera.

PEPT experiments involve placing the equipment of interest within the field-of-view (FOV) of a positron-sensitive detector. Commonly, these detectors correspond to repurposed PET cameras from hospitals, with FOV not greater than the space required for a patient to fit through the bore, *i.e.* under 0.15 m^3 or 0.8 m^2 by 0.15 m deep. However, some experimental equipment will not fit within the FOV of existing detectors. To address this challenge, a large modular array of detectors, called LaMA, has been recently designed at the University of Birmingham Positron Imaging Centre (PIC) to be assembled around experimental systems in custom geometries (Parker et al., 2022; Herald et al., 2023).

This work presents an experimental study aimed at quantifying the fluid dynamics of a 2 m tall fluidised bed flotation cell using PEPT. The LaMA detector was assembled around the geometry of the experimental system in a custom configuration, which enabled the imaging of a large-scale laboratory prototype of the cell. To the authors' knowledge, this is the largest PEPT experiment to date in terms of the height of the field-of-view. The objective of this study is to investigate the complex fluid dynamics of the fluidised bed flotation cell, which plays a critical role in the separation of coarse mineral particles.

2. Materials and methods

2.1. CoarseAIR fluidised bed flotation cell – laboratory-scale prototype

The experiments were performed using the CoarseAIR™-100 (CA100), a 2.3 m high fluidised bed flotation cell with a capacity of just under 20 L, as depicted in Fig. 1. The CoarseAIR™ cell, based on the REFLUX™ classifier design (Galvin et al., 2016), comprises a lower fluidised bed and an upper system of inclined channels called lamella plates. Small air bubbles are generated by injecting pressurised air into the fluidisation water. The feed suspension is injected at an intermediate height. The whole tank experiences a positive water bias, with small/light particles flowing upwards through the inclined channels, whereas the larger/heavier particles sink into the lower fluidised bed. Hydrophobic particles attach to the bubbles, forming bubble-particle clusters with low apparent density, and thus collect towards the top of the cell. Further details about the cell design and metallurgical performance can be found in Crompton et al. (2022).

The cell was operated semi-continuously, with an initial batch of mineral pulp feed. The tailings were recycled, while the concentrate was collected into a separate tank, being filtered to recycle the fluidisation water. High-pressure air was injected at 80 PSI into the fluidisation water to produce small bubbles. Symmetric inlets introduced the aerated fluidisation water into the fluidisation chamber at the bottom of the cell (see Fig. 1(a)). The cell included instrumentation for adjusting fluidisation and airflow rates, providing control over the operating conditions.

2.2. Large Modular Array (LaMA) for PEPT

The Large Modular Array (LaMA) is a flexible, geometrically reconfigurable PEPT system developed upon the CTI/Siemens ECAT PET scanner architecture. The system was first tested and assembled in the late 2000s at the PIC (Parker et al., 2008) but only consisted of 16 buckets or modules based on the ECAT 931 scanner. Soon afterwards, it was fitted with parts from the upgraded ECAT 951 scanner and did not undergo any major development until its major expansion and modification in 2021.

Today the array consists of 48 buckets based on the 951 series detectors and electronics which can interface with one of the two available independent coincidence processors (CP), one from ECAT 951 and one from ECAT 931. Each bucket is contained within a square aluminium enclosure measuring 360 mm wide, 95 mm tall, and 460 mm deep and contains four bismuth germanate (BGO) scintillator detector blocks spaced 88 mm apart, centred upon the front face of the bucket as shown in Fig. 2. Each detector block crystal is approximately 50×50 mm^2 in area and 30 mm thick, subdivided into an 8×8 array of crystal elements, and is viewed by four photomultiplier tubes. The 951 series bucket controller then processes the output from each of the photomultiplier tubes for each of the four detector blocks to determine within which crystal element the gamma ray has interacted. These positional data are then sent to the CP to determine if an interaction has occurred in any of the other buckets within the 12 ns coincidence resolving time.

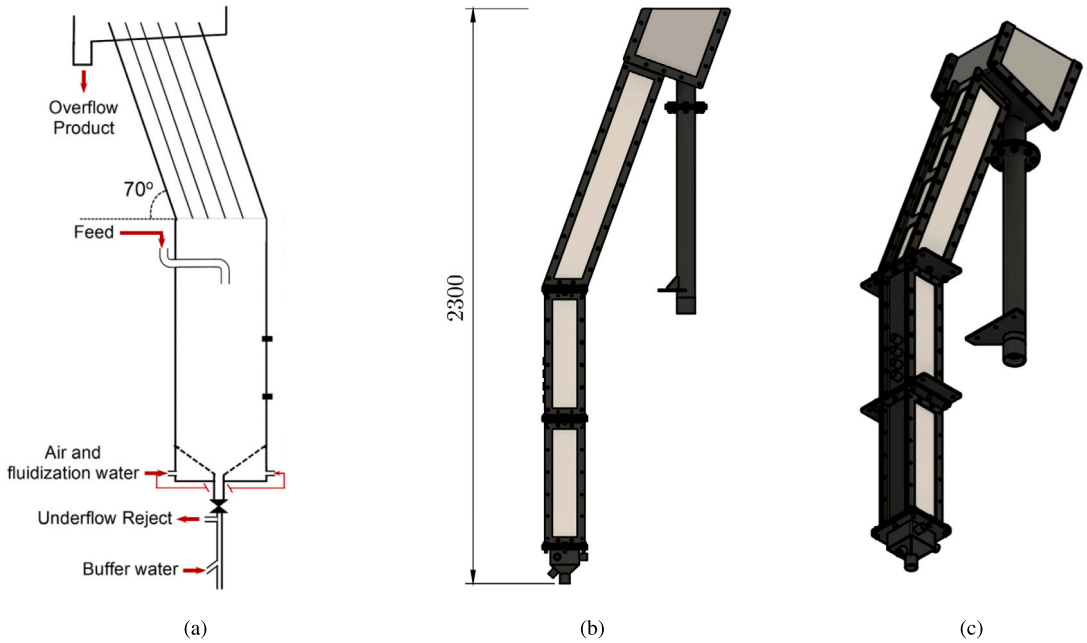

Fig. 1. Schematic of the CoarseAIR™ fluidised bed flotation cell, showing (a) the main sections, inlets and outlets (adapted from Crompton et al. (2022)), (b) a lateral view of the cell, and (c) an isometric view of the laboratory-scale prototype used in this work. The box at the bottom is the fluidisation chamber, where a mix of water and air is injected at high pressure. The vertical section is the fluidised bed and the slanted section hosts lamella plates that aim to improve the separation efficiency.

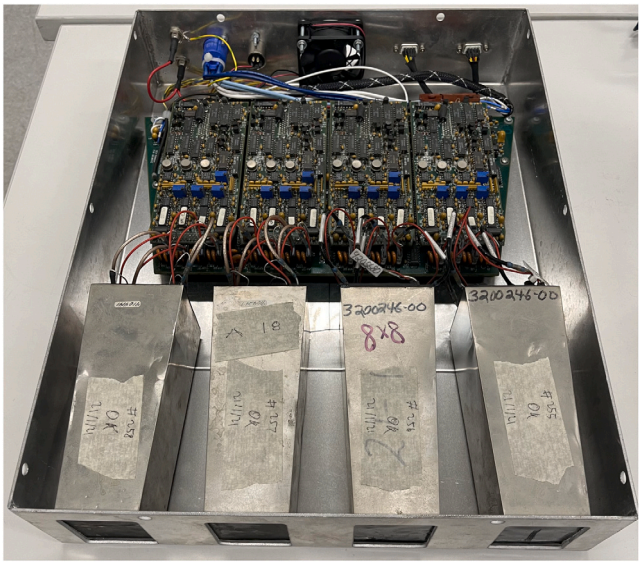

Fig. 2. A LaMA bucket with its lid removed displaying four detector blocks and a bucket controller board from the ECAT 951 PET scanner.

To use all of the 48 buckets, two CPs are used as each one can only accept inputs from 2 to 32 buckets. Therefore, the buckets can be distributed between the two CPs according to the experiment's geometrical requirements. The coincidence data are then recorded from each CP by custom-designed acquisition boards that also add a timestamp to each event. This timestamp allows the data produced by the two CPs to be combined during post-processing to continuously track the movement of a tracer as it travels between the areas viewed by each of the CPs. Therefore, this extends the FOV of the system beyond what is possible with just a single scanner's worth of electronics.

Due to the modular nature of the array, LaMA can be built after the equipment is set up to closely surround it and follow any awkward geometry. To view the full 2.3 m tall fluidised bed flotation cell, a flat plane design was chosen where the buckets were stacked in two tall columns exactly 500 mm apart, as seen in Fig. 5(b). The fluidisation chamber, fluidised bed, and its intersection with the angled lamella plates were viewed by 32 buckets connected to the 951 series CP and the remaining upper lamella plates were viewed by 16 buckets connected to the 931 series CP. This bucket arrangement essentially divided the system into two sections. The first section provided accurate particle tracking within the fluidised bed and at the lamellae intersection while the second section further extended the FOV to include the rest of the lamellae. The whole arrangement was supported by a custom-designed frame made to follow the angled lamellae of the cell built from aluminium profile extrusions, as shown in Fig. 5(c).

2.3. Materials and reagents

Copper tailings were used as the mineral feed, sourced by FLSmidth. The tailings received were sieved and deslimed, discarding the fraction under 75 μm. After desliming, the P80 of the sample was 250 μm, as shown in Fig. 3. A 50:50 mixture of MIBC and X133 was used as frother. PAX and diesel were used as the copper-ore collectors.

2.4. PEPT tracers

For these measurements directly activated tracers were used. The activation was performed using an 11.2 MeV proton beam at the Birmingham Cyclotron Facility (Anon; Parker and Wheldon, 2018). The chalcopyrite particles were prepared at the Positron Imaging Centre at the School of Physics and Astronomy in Birmingham, which is in the same building as the Cyclotron and used straight after the irradiation for the measurements. The technique of directly activated tracers for PEPT is outlined in Fan et al. (2006). The activated chalcopyrite particles were dispersed in a concentrated solution of collectors (PAX + diesel) and utilised as proxies for hydrophobic (valuable) particles. When the chalcopyrite particles were directly introduced into the cell without any treatment in collectors, they behaved as hydrophilic (gangue) particles (see Fig. 4).

The chalcopyrite particles used as tracers had a specific gravity of 4200 and varied in diameter, ranging between 300 to 700 μm. The activity of the tracers used ranged between 2.5 to 4.5 MBq.

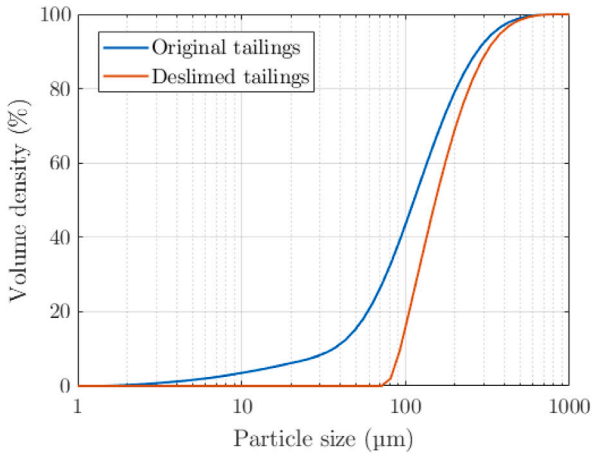

Fig. 3. Particle size distribution of the tailings material. The blue line represents the cumulative distribution by volume of the tailings as received, and the orange line represents the particle size distribution after desliming. (For interpretation of the references to colour in this figure legend, the reader is referred to the web version of this article.)

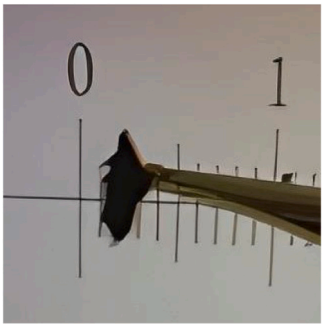

Fig. 4. Chalcopyrite particles were directly activated to be used as tracers. The particles we used as hydrophobic and hydrophilic tracers, depending on their treatment with collectors.

Table 1
Operating conditions assessed in PEPT tests. Superficial gas velocity (J_G) and superficial water velocity of fluidisation (J_{W_f}) were varied at three levels.

Operating condition	J_G (cm/s)	J_{W_f} (cm/s)
Low	0.11	0.13
Normal	0.17	0.19
High	0.23	0.25

2.5. Experimental procedure

PEPT experiments were conducted utilising LaMA for particle tracking as shown in Fig. 5. Experiments were duplicated on different days, using different tracers and material feed. Each experiment used only one tracer at a time, testing hydrophobic and hydrophilic tracers.

The airflow and fluidisation rates were set constant for most of the experiments, with a superficial gas velocity (J_G) of 0.17 cm/s and a superficial water velocity of fluidisation (J_{W_f}) of 0.19 cm/s, following the "Normal" operating conditions defined by FLSmidth (see Table 1). Airflow and fluidisation rates were also varied to assess the effect of these operating conditions on the fluid dynamics of the system. These variability tests, however, were only performed for hydrophilic tracers, as tracer recirculation allowed for longer experiments to be run.

A feed with a solid content of 50%$_{w/w}$ was prepared in an external agitated tank, using 3 kg of tailings samples 100% ≥ 75 µm and 3 litres of tap water. The pulp was conditioned by adding 10 g/t of diesel and agitating for 5 min, followed by the addition of 90 g/t of PAX and 3 min of agitation. Finally, 40 g/t of the frother mix was added to the pulp. The conditioned pulp was injected into the CA100 cell from the middle injection point using a peristaltic pump. The fluidisation water tank was conditioned with the frother mix at a dosage of 20 ppm$_{v/v}$. Fig. 6 presents a schematic representation of the process flow diagram used during experiments.

The positron-emitting tracers were recovered at the end of each experiment. On the occasions when the tracer overflowed with the concentrate (hydrophobic tracers), these were recovered by placing a sieve in the concentrate pipe, being manually re-injected into the cell for further testing. Conversely, when the tracer reported to the tailings, it was recycled back into the cell by the peristaltic pumps.

2.6. PEPT data analysis using PEPT-ML

The experimental PEPT data were analysed using the machine learning-based algorithm PEPT-ML, proposed by Nicuşan and Windows-Yule (2020) to determine the position of the tracer for each of the detected positron annihilation events. In this algorithm, the data is split into a series of individual samples, each containing a given N number of LORs. For every sample of LORs, PEPT-ML computes cutpoints or the midpoint of the shortest line segment that is perpendicular to a pair of LORs for every possible pair of LORs in a sample that is also shorter than a set maximum distance. These cutpoints are then clustered using a Hierarchical Density-Based Spatial Clustering of Applications with Noise (HDBSCAN) algorithm, and the centres of the clusters are extracted in so-called "1-pass clustering". These centres can then be further split into samples of a given size and clustered again using the HDBSCAN algorithm in "2-pass clustering". The trajectory of every particle using the centres from the previous step is then constructed.

When extracting post-processed data from tracer trajectories, it is often important to sample data at fixed timesteps. Being a Lagrangian technique, PEPT tracers can be located more frequently in more sensitive areas of the FOV of a PEPT camera, especially in LaMA where sensitivity varies due to the spaces between the detector blocks. Therefore, it is necessary to use interpolation to convert the "randomly" sampled positions into regular timesteps. These interpolated tracks are then used to calculate the tracer velocity.

All individual tracks were analysed, quantifying the motion and velocity of the tracers. Representative two-minute tracks of each tracer are shown and discussed in Section 3.1, while Section 3.2 focuses on particle dynamics in the slanted lamella plates.

Over one hour of PEPT data was used to create a time-averaged 3D Eulerian grid with voxel dimensions of 10 mm by 10 mm by 10 mm. Slanted voxels were used in the lamella plates' region for consistency. The central slice of the cell, represented by all the voxels in the yz plane with $x \in [-10, 10]$ mm, was analysed in Section 3.3, focusing on the vertical velocity and the residence time in terms of passes. For the velocity data, its different vectorial components for each voxel were represented by a kernel-smoothed distribution, as described in Mesa et al. (2021) and Cole et al. (2022a). The peak of the distribution, representing the most likely velocity, was used as the representative value for each voxel, eliminating the effect of outliers. The measurement of passes refers to the number of times the tracer passed through a voxel (relative to entering and exiting the cell), normalised by the passes in the slice (Mesa et al., 2022).

3. Results and discussion

3.1. Analysis of individual tracks

Representative two-minute tracks, one for each tracer type, are discussed in this section. Fig. 7 shows the position with time of the tracer on each Cartesian component, where x represents the depth of the cell (ranging between −50 and 50 mm), y represents the vertical direction (between 0 and 2100 mm) and z the horizontal component

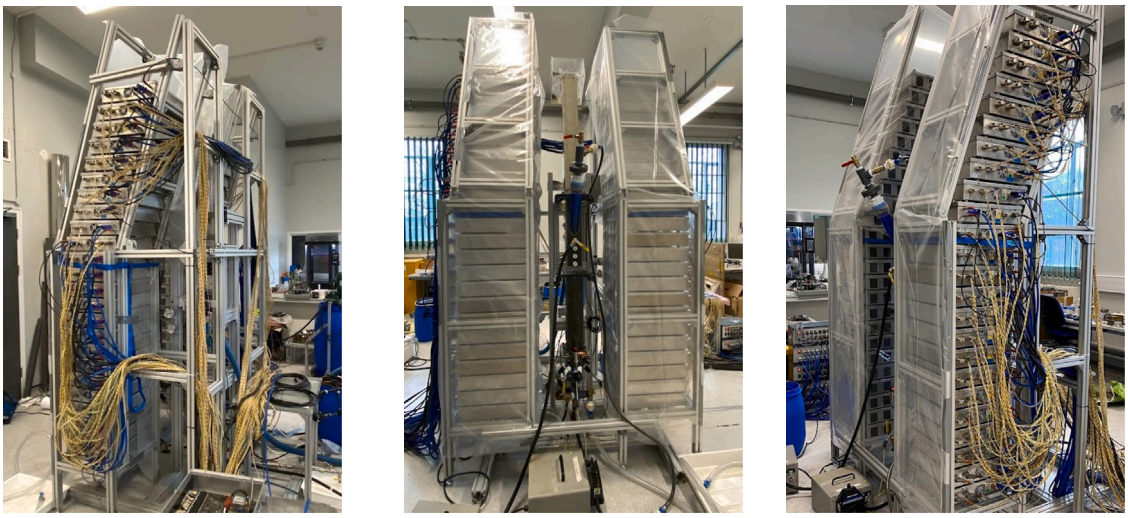

(a) (b) (c)

Fig. 5. Large Modular Array (LaMA) for PEPT in an ad-hoc configuration for the CoarseAIR™ fluidised bed experiments. Photographs obtained during experiments in the Positron Imaging Centre at the University of Birmingham.

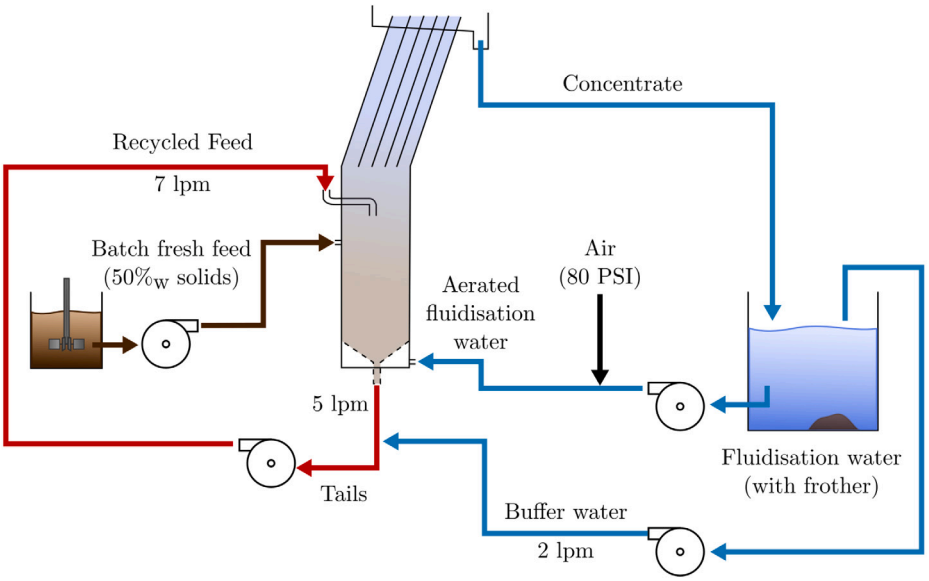

Fig. 6. Process flow diagram of the CA100™ setup for continuous PEPT experiments.

(−300 to 50 mm). The tracers were fed into the cell at a height of $y \approx$ 1000 mm. The tracers would move within the cell and finally would either overflow as a concentrate or sink towards the tailings.

The configuration of LaMA, as described in Section 2.2, was such that two groups of cameras were used. This separation of LaMA into two sections is evidenced in Fig. 7(a) in the slight gap between the tracks when crossing a height of $y \approx$ 1500 mm (close to 60 s on the track). The hydrophobic tracer shown in Fig. 7(a) floated and reported to the concentrate after approximately 90 s. The tracer was then sieved from the concentrate using a Geiger counter to identify its location and fed back into the cell for further testing.

The hydrophilic tracers, on the other hand, were recycled from the tailings back into the cell, allowing long experiments to be performed. In the particular two-minute track shown in Fig. 7(b), it is observed that on most occasions the hydrophilic tracer sunk directly to the tailings for recycling. However, between the times 30–110 s, it can be observed that the hydrophilic tracer was suspended in the cell, even rising back near the injection point, before sinking and recirculating again.

Fig. 8 shows the velocity Cartesian components of the tracer motion. The highest velocities were reached on the vertical axis y, as expected, achieving speeds close to 400 mm/s. The vertical velocity can be directly linked to the upward motion related to the rise of a tracer attached to a bubble or the sinking motion of a gangue particle, thus most attention has been paid to this component of the overall velocity.

To better understand the motion and velocity of the tracks, a 2D representation (yz plane) is shown in Fig. 9. The motion of the tracer is represented by the track, and the colour of the line represents the vertical velocity.

The hydrophobic tracer shown in Fig. 9(a) entered the cell and circulated in the upper section of the columnar body, with fluctuating vertical speeds below 400 mm/s. At around one minute of tracking, the hydrophobic tracer was collected towards the lamella plates. In the lamella plates, the tracer reached a vertical velocity of 200 mm/s, with fluctuating velocities in the x and z directions. The motion within the lamella plates is further explored in Section 3.2.

In the case of the hydrophilic tracer, Fig. 9(b) evidences a rapid downward movement near the wall near the injection point, as the

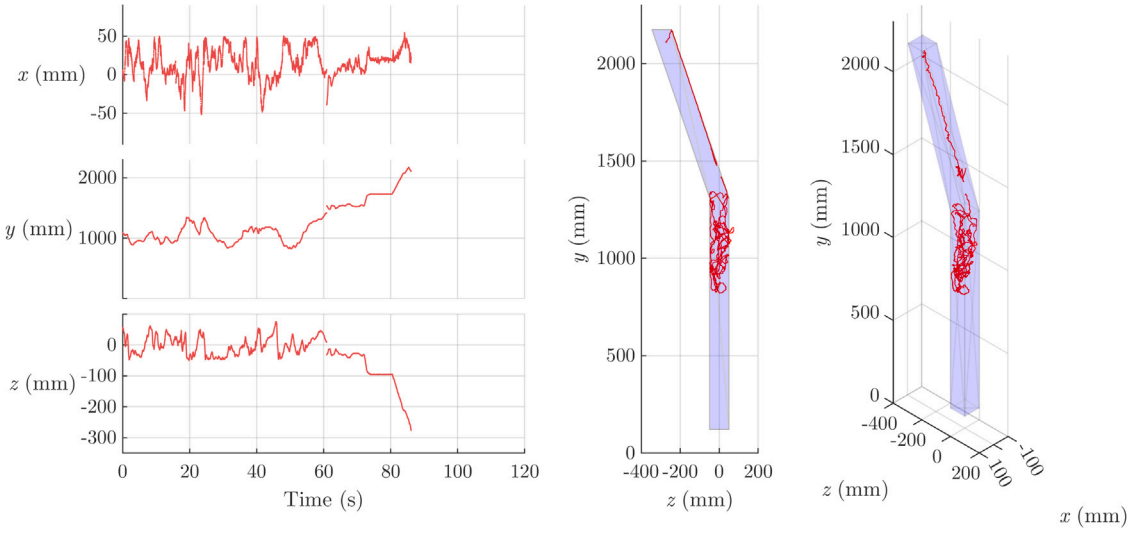

(a) Hydrophobic tracer

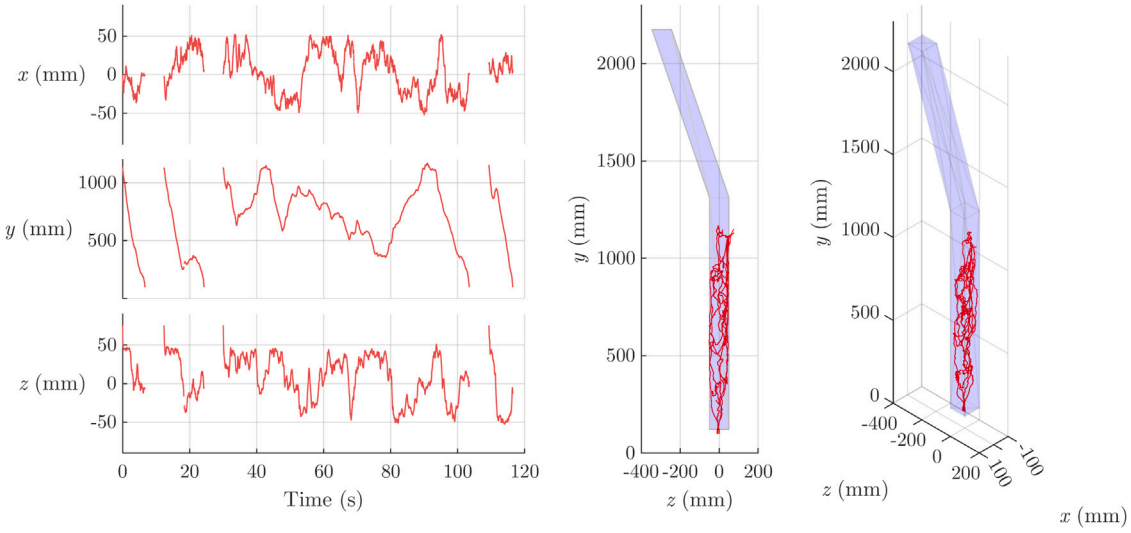

(b) Hydrophilic tracer

Fig. 7. Representative two-minute tracks of flotation with (a) a hydrophobic and (b) a hydrophilic tracer.

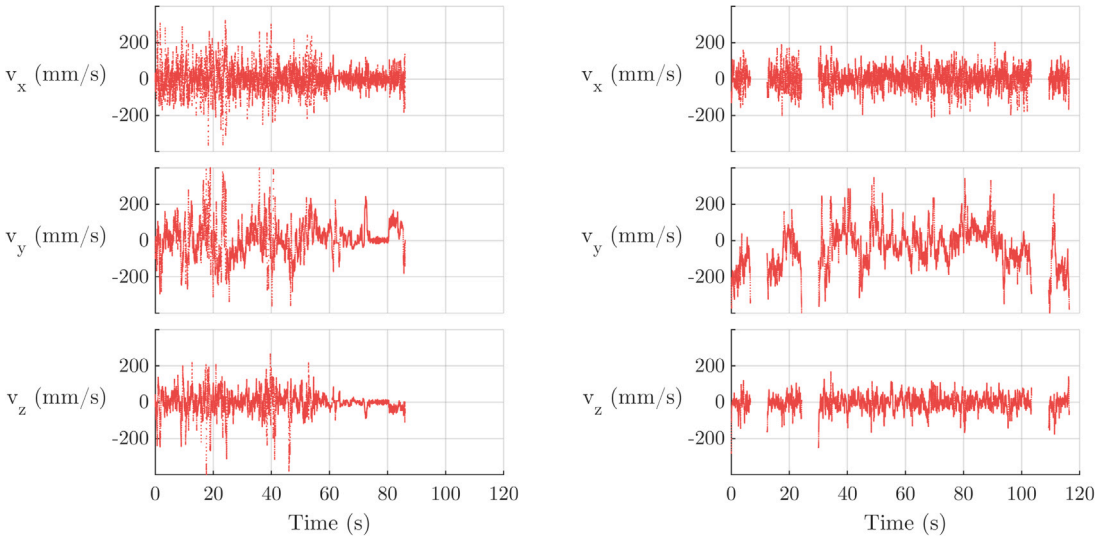

(a) Hydrophobic tracer

(b) Hydrophilic tracer

Fig. 8. Velocity components of the representative two-minute tracks obtained with (a) a hydrophobic and (b) a hydrophilic tracer.

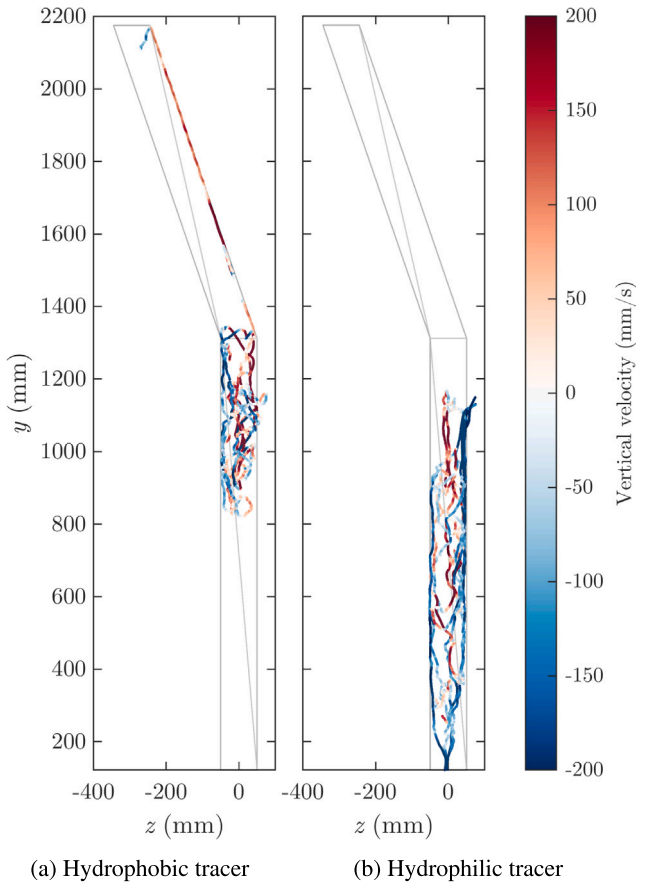

(a) Hydrophobic tracer (b) Hydrophilic tracer

Fig. 9. Lateral view of the representative two-minute tracks obtained with (a) hydrophobic and (b) hydrophilic tracer. The vertical velocity $\vec{v}_y$ is represented by the colour bar. (For interpretation of the references to colour in this figure legend, the reader is referred to the web version of this article.)

recirculating flow is injected with a downward angle at a high velocity. In the two minutes tracked, the hydrophilic tracer recirculated four times, with a residence time of under one minute. The third time the tracer entered the cell in this 2-minute track, it had a longer residence time, circulating within the columnar section of the cell, reaching positive vertical velocities of 300 mm/s.

The analysis of multiple tracks such as those shown in Figs. 7 to 9 suggests that the hydrophilic particles moved predominantly downward, with a short residence time. This effect could imply that the design of the recirculation inlet of this laboratory-scale CA100, combined with the operation of the recirculation pump, had a direct effect on the operation of the cell, altering the stability of the fluidised bed. Similarly, the analysis of multiple hydrophobic tracks shows that coarse valuable particles are quickly floated by the CA100. Generalised observations of flow patterns are discussed in Section 3.3, where long tracks are analysed using Eulerian representations.

3.2. Particle motion in the lamella plates

Multiple tracks obtained with hydrophobic tracers are shown in Fig. 10. These tracks correspond to approximately 15 min of operation, obtained during independent experimental runs on two different days, with different tracers.

Once a hydrophobic particle entered the lamella plates, its movement in the component z was controlled by the spacing between plates. The motion in the xy plane, however, denoted a tortuous path towards the top of the cell. The central subfigure in Fig. 10, shows that the tracer did not move in a straight line upward once it entered the lamella plates. On the contrary, the tracer covered most of the available width of the cell (x component), evidencing downward motion near the walls.

The tortuosity of each track in the lamella plates region was calculated as the ratio between the 3D arc-length of the track and the Eulerian distance between the points of entry and overflow. Consequently, a tortuosity value of 1 would represent a straight path in the region between two lamella plates, while values over 1 represent more convoluted tracks. The average path tortuosity in the lamella plates was 7.3, ranging between 2 and 19. Tortuosity variability may have been caused by differences in tracer size and shape, subtle geometrical differences between lamella plates, or differences in the size and number of bubbles to which the tracer was attached.

3.3. Eulerian representation analysis

For the analysis of the time-averaged velocity data, the tracer velocity ($\vec{v}$) was decomposed into its vectorial components, namely the depth ($\vec{v}_x$), vertical ($\vec{v}_y$) and horizontal ($\vec{v}_z$) velocities, and were represented by the peak of the velocity distribution in each voxel. Eulerian representations of the vertical velocities of the hydrophilic and hydrophobic tracers are shown in Fig. 11. The central slices in depth ($x \in [-10, 10]$ mm) were chosen as these are farther away from the walls, allowing the analysis of bulk behaviour. This slice effectively entails the merging of two yz slices of 10 mm thickness ($x \in [-10, 0] \cup [-10, 0]$ mm), which is possible due to the symmetry of the flotation cell along the vertical dimension, allowing to increase the number of data points within each voxel (Mesa et al., 2021).

Fig. 11(a) shows that hydrophobic particles move throughout the whole cell until they attach to a bubble and are collected towards the lamella plates. As observed in Section 3.1, the tracer tends to rise near the centre of the cell and sink near the walls, which may be an indication of convective flows in the cell. In this central slice, it is observed that the hydrophobic particles tend to ascend using only the central lamella plates.

In the case of hydrophilic particles (Fig. 11(b)), the velocity profile evidences a rapid downward movement near the wall closer to the injection point, as the recirculating flow is injected downward at high velocity. Therefore, it is plausible that the design of the recirculation inlet combined with the operation of the recirculation pump directly affects the operation of the cell, altering the stability of the fluidised bed. As in the case of hydrophobic particles, an upward motion is observed in the middle of the cell, which is related to the fluidisation water injection from the bottom.

Notably, in over one hour of continuous operation, the hydrophilic tracer was never wrongly recovered, which translates to a great selectivity. Admittedly, this observation, based on a coarse hydrophilic tracer, can only be extended to similarly coarse hydrophilic particles, while finer gangue could well be subject to entrainment into the lamellae plates. Furthermore, and despite the large size of the tracers used (> 300 μm), the hydrophobic tracer rarely reported to tailings, implying that high recoveries can be achieved with CA100. These metallurgical observations are well aligned with the results obtained by Crompton et al. (2023) with the CA100, where a cumulative recovery of over 80% was reported for valuable particles ≤ 600 μm.

The normalised passes of the tracers per each voxel are shown in Fig. 12. The hydrophobic particles (Fig. 12(a)) tend to circulate several times in the upper section of the columnar body, presenting a relatively uniform occupancy. The number of passes in the lamella plates is considerably lower, implying that once tracers entered into this slanted section, they tended to move upwards relatively fast, despite the tortuosity described in Section 3.2. Notably, the hydrophobic tracers only used the central and top lamella plates, which could be related to an effect of the feed/recirculation flow displacing the ascending particles towards the opposite wall.

The hydrophilic tracer (Fig. 12(b)) shows a higher pass count at the bottom of the tank. This behaviour evidences that, although large hydrophilic particles tend to move downwards, there is still mixing and suspension of these particles due to the fluidisation water.

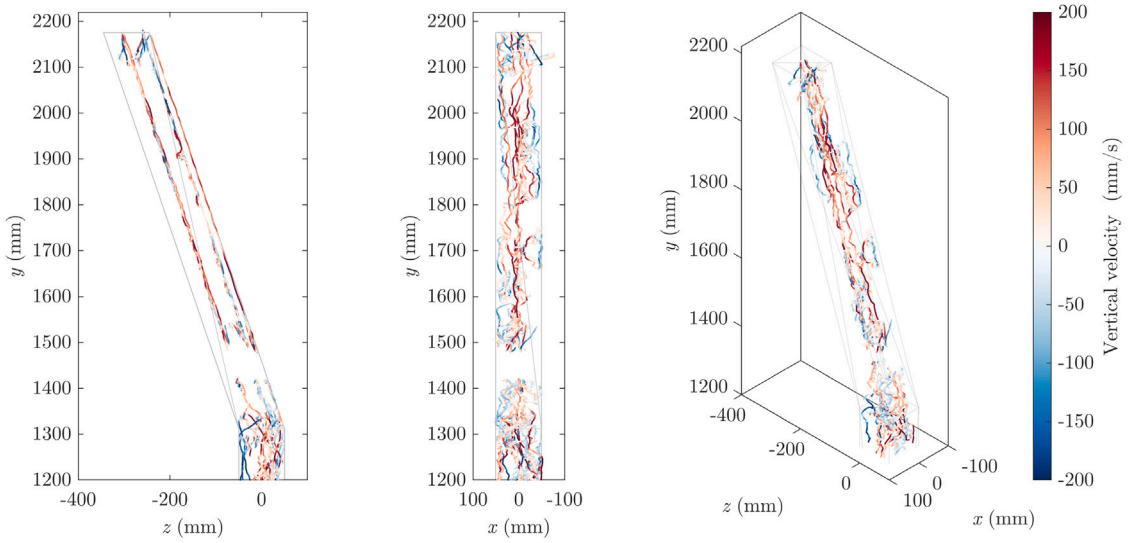

Fig. 10. Particle dynamics in the inclined lamella plates.

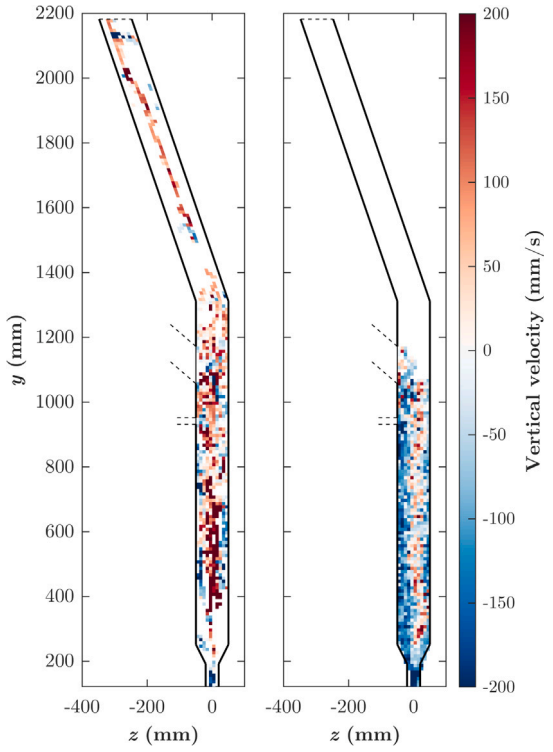

(a) Hydrophobic tracers (b) Hydrophilic tracers

Fig. 11. Eulerian representation of the time-average vertical velocity of (a) hydrophobic and (b) hydrophilic particles. The Eulerian representations considered multiple tracks, with a voxel size of 10 mm by 10 mm by 10 mm, sliced in the middle plane of the cell ($x \in [-10, 10]$ mm).

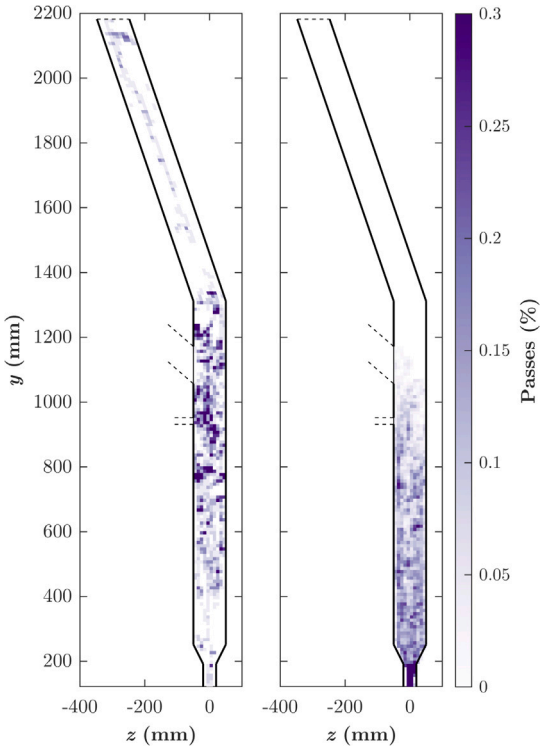

(a) Hydrophobic tracers (b) Hydrophilic tracers

Fig. 12. Eulerian representation of the time-average Location density of (a) hydrophobic and (b) hydrophilic particles. The Eulerian representations considered multiple tracks, with a voxel size of 1 cm^3, sliced at the middle plane of the cell ($x \in [-10, 10]$ mm).

3.4. Effect of operating conditions

Three different operating conditions were tested for the hydrophilic tracers, varying the airflow and fluidisation rate, into "Low", "Normal" and "High", as described in Table 1. The results obtained are shown in Fig. 13. The effect of operating conditions on the motion of hydrophobic tracers was not included, due to their short residence time (Fig. 7(a)) and the difficulties associated with tracer recovery from the concentrate. Future work could consider the use of multiple hydrophobic tracers (M-PEPT (Wiggins et al., 2019)) to increase the data obtained per experiment, allowing for the testing of a wider range of operating conditions.

Although the overall behaviour of the hydrophilic tracer for the different operating conditions is similar in terms of motion, some differences can be appreciated, both in terms of vertical velocity values and the occupied zones. At the highest airflow and fluidisation rates tested (Fig. 13(c)), the hydrophilic particles evidenced a faster upward motion in the centre of the tank. Moreover, this upward flow occupied

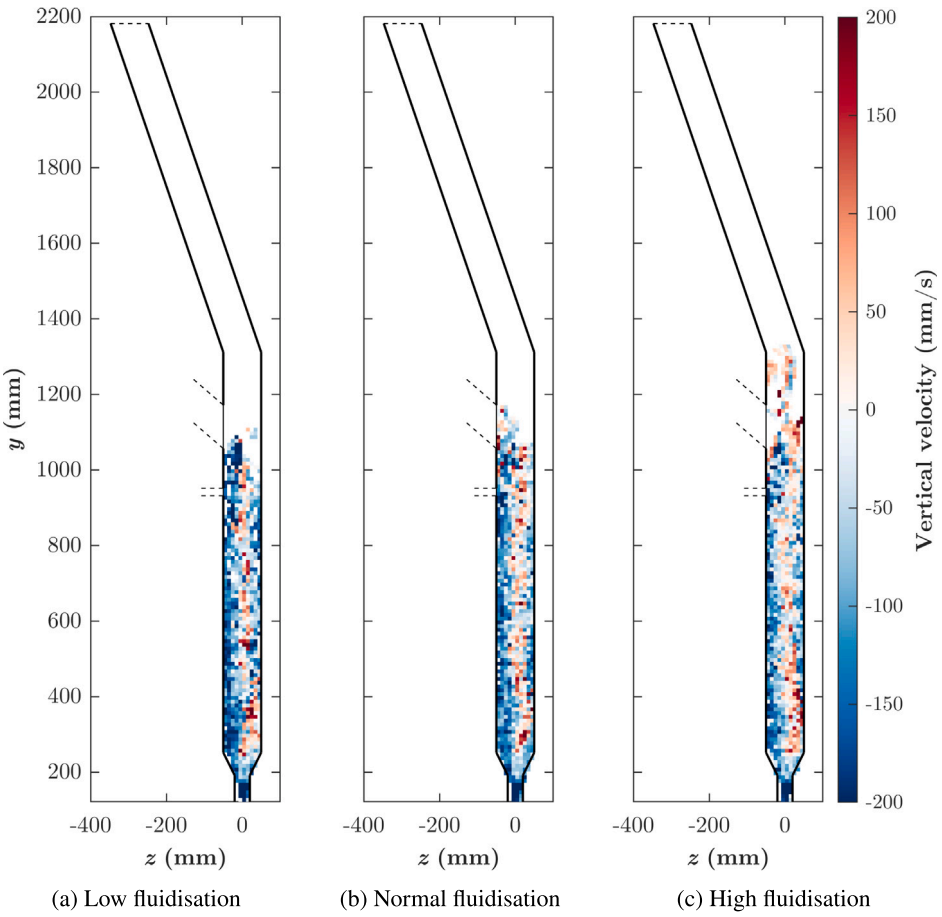

Fig. 13. Effect of the operating conditions on the vertical velocity of the hydrophilic tracers, shown in time-averaged Eulerian representations of the middle plane of the cell ($x \in [-10, 10]$ mm). The operating conditions correspond to (a) Low fluidisation: $J_G = 0.11$ cm/s and $J_{W_f} = 0.13$ cm/s, (b) Normal fluidisation: $J_G = 0.17$ cm/s and $J_{W_f} = 0.19$ cm/s, and (c) High fluidisation: $J_G = 0.23$ cm/s and $J_{W_f} = 0.25$ cm/s.

a larger portion of the tank when compared to the normal operating conditions (Figs. 11(b) and 13(b)), while also reaching higher into the tank, closer to the lamella plates.

A lower fluidisation Fig. 13(a), on the other hand, resulted in a more pronounced downward motion dominating the behaviour of hydrophilic particles. The level of the bed seems to have been affected as well, reaching a lower level than in normal conditions, although the difference is less pronounced than in the case of High v/s Normal comparison.

4. Conclusions

This study represents a substantial advancement in our understanding of the fluid dynamics of fluidised bed flotation cells (FBFCs), specifically focusing on the CoarseAir™-100. The Large Modular Array (LaMA) PEPT system was used to perform the largest positron emission particle tracking experiment to date, shedding light on the complex fluid dynamics within large-scale fluidised bed flotation cells.

The study allowed us to carry out a quantitative assessment of the flotation of hydrophobic tracers as they preferentially floated towards the concentrate despite their coarse size, while hydrophilic tracers exhibited a distinctive recycling mechanism, moving from tailings back into the cell. Detailed Cartesian tracking of individual particle paths unveiled intricate motion patterns within the system. The analysis of hydrophobic tracer dynamics within the inclined lamella plates revealed tortuous paths, emphasising the significant influence of design and geometry on particle movement.

Decomposing time-averaged velocity data through Eulerian representation provided further insights into the behaviour of hydrophobic and hydrophilic particles. Hydrophobic particles moved throughout the cell, displaying an ascending motion primarily through central and top lamella plates. In contrast, hydrophilic particles exhibited rapid downward and upward movements, reflecting the impact of operating conditions on fluidisation dynamics.

Exploration of different operating conditions highlighted the variations in the behaviour of hydrophilic tracers. Higher airflow and fluidisation rates accentuated upward motion, expanding the occupancy of hydrophilic particles in the central region of the tank.

This work significantly contributes to the knowledge base of fluidised bed flotation cells. The acquired experimental data not only enhance our understanding of particle dynamics but also provide a benchmark for validating multiphase simulations and evaluating alternative designs.

CRediT authorship contribution statement

Diego Mesa: Writing – original draft, Visualization, Software, Methodology, Investigation, Formal analysis, Data curation. **Dawid M. Hampel:** Writing – original draft, Visualization, Software, Methodology, Formal analysis, Data curation. **Stephen J. Neethling:** Resources, Project administration, Funding acquisition. **Tzany Kokalova Wheldon:** Writing – review & editing, Supervision, Resources, Project administration, Methodology, Conceptualization. **Pablo R. Brito-Parada:** Writing – review & editing, Supervision, Resources, Project administration, Funding acquisition, Conceptualization.

Declaration of competing interest

The authors declare the following financial interests/personal relationships which may be considered as potential competing interests: Pablo Brito-Parada reports financial support was provided by FLSmidth Inc. Co-author Pablo Brito-Parada is Editor-in-Chief of Minerals Engineering journal. The rest of the authors declare that they have no known competing financial interests or personal relationships that could have appeared to influence the work reported in this paper.

Data availability

Data will be made available on request.

Acknowledgements

The authors acknowledge funding from FLSmidth, Denmark. The authors thank Mr. Yui Ming Kan, technician at the Positron Imaging Centre, for his help during the experiments. The authors also thank Dr Ben Phoenix and the Birmingham Cyclotron team for their help with the direct activation of the tracers used.

References

Anon, MC40 cyclotron facility - The Birmingham Centre for Nuclear Education and Research, University of Birmingham, URL https://www.birmingham.ac.uk/research/activity/nuclear/about-us/facilities/mc40-cyclotron-facility.aspx.

Chelgani, S. Chehreh, Parian, M., Parapari, P. Semsari, Ghorbani, Y., Rosenkranz, J., 2019. A comparative study on the effects of dry and wet grinding on mineral flotation separation–a review. J. Mater. Res. Technol. (ISSN: 2238-7854) 8 (5), 5004–5011. http://dx.doi.org/10.1016/j.jmrt.2019.07.053, URL https://www.sciencedirect.com/science/article/pii/S223878541930849X.

Cole, K., Barker, Daniel J., Brito-Parada, Pablo R., Buffler, Andy, Hadler, Kathryn, Mackay, Isobel, Mesa, Diego, Morrison, Angus J., Neethling, Stephen, Norori-McCormac, Alexander, Shean, Barry, Cilliers, Jan, 2022a. Standard method for performing positron emission particle tracking (PEPT) measurements of froth flotation at PEPT Cape Town. MethodsX (ISSN: 2215-0161) 101680. http://dx.doi.org/10.1016/j.mex.2022.101680, URL https://www.sciencedirect.com/science/article/pii/S2215016122000644.

Cole, K., Brito-Parada, Pablo R., Hadler, Kathryn, Mesa, Diego, Neethling, Stephen J., Norori-McCormac, Alexander M., Cilliers, Jan J., 2022b. Characterisation of solid hydrodynamics in a three-phase stirred tank reactor with positron emission particle tracking (PEPT). Chem. Eng. J. (ISSN: 1385-8947) 433, 133819. http://dx.doi.org/10.1016/j.cej.2021.133819, URL https://www.sciencedirect.com/science/article/pii/S1385894721053924.

Crompton, Luke J., Islam, Md. Tariqul, Galvin, Kevin P., 2022. Investigation of internal classification in coarse particle flotation of chalcopyrite using the CoarseAIRTM. Minerals (ISSN: 2075-163X) 12 (6), 783. http://dx.doi.org/10.3390/min12060783, URL https://www.mdpi.com/2075-163X/12/6/783, Number: 6 Publisher: Multidisciplinary Digital Publishing Institute.

Crompton, Luke J., Islam, Md. Tariqul, Galvin, Kevin P., 2023. Assessment of the partitioning of coarse hydrophobic particles in the product concentrate of the CoarseAIR™ flotation system using a novel mechanical cell reference method. Miner. Eng. (ISSN: 0892-6875) 198, 108088. http://dx.doi.org/10.1016/j.mineng.2023.108088, URL https://www.sciencedirect.com/science/article/pii/S0892687523001024.

Deniz, V., 2013. Comparisons of dry grinding kinetics of lignite, bituminous coal, and petroleum coke. Energy Sources A (ISSN: 1556-7036) 35 (10), 913–920. http://dx.doi.org/10.1080/15567036.2010.514591, Publisher: Taylor & Francis _eprint.

Dickinson, J.E., Galvin, K.P., 2014. Fluidized bed desliming in fine particle flotation – Part I. Chem. Eng. Sci. (ISSN: 00092509) 108, 283–298. http://dx.doi.org/10.1016/j.ces.2013.11.006, URL https://linkinghub.elsevier.com/retrieve/pii/S0009250913007355.

Fan, X., Parker, D.J., Smith, M.D., 2006. Labelling a single particle for positron emission particle tracking using direct activation and ion-exchange techniques. Nucl. Instrum. Methods Phys. Res. A (ISSN: 0168-9002) 562 (1), 345–350. http://dx.doi.org/10.1016/j.nima.2006.03.015, URL https://www.sciencedirect.com/science/article/pii/S0168900206005341.

Fosu, Shadrack, Awatey, Bellson, Skinner, William, Zanin, Massimiliano, 2015. Flotation of coarse composite particles in mechanical cell vs. the fluidised-bed separator (The HydroFloat™). Miner. Eng. (ISSN: 0892-6875) 77, 137–149. http://dx.doi.org/10.1016/j.mineng.2015.03.011, URL https://www.sciencedirect.com/science/article/pii/S0892687515001016.

Galvin, K.P., Dickinson, J.E., 2014. Fluidized bed desliming in fine particle flotation – Part II: Flotation of a model feed. Chem. Eng. Sci. (ISSN: 0009-2509) 108, 299–309. http://dx.doi.org/10.1016/j.ces.2013.11.027, URL https://www.sciencedirect.com/science/article/pii/S000925091300763X.

Galvin, K.P., Harvey, N.G., Dickinson, J.E., 2014. Fluidized bed desliming in fine particle flotation – Part III flotation of difficult to clean coal. Froth Flotation, Miner. Eng. (ISSN: 0892-6875) Froth Flotation, 66–68, 94–101. http://dx.doi.org/10.1016/j.mineng.2014.02.008.URL https://www.sciencedirect.com/science/article/pii/S0892687514000557,

Galvin, K.P., Zhou, J., Price, A.J., Agrwal, P., Iveson, S.M., 2016. Single-stage recovery and concentration of mineral sands using a REFLUX™ classifier. Miner. Eng. (ISSN: 0892-6875) 93, 32–40. http://dx.doi.org/10.1016/j.mineng.2016.04.010, URL https://www.sciencedirect.com/science/article/pii/S0892687516301029.

Hamidipour, Mohsen, Chen, Jinwen, Larachi, Faïçal, 2012. CFD study on hydrodynamics in three-phase fluidized beds—Application of turbulence models and experimental validation. Chem. Eng. Sci. (ISSN: 0009-2509) 78, 167–180. http://dx.doi.org/10.1016/j.ces.2012.05.016, URL https://www.sciencedirect.com/science/article/pii/S0009250912002977.

Han, Jikang, Liu, Taishan, Li, Yanfeng, Chen, Peng, Yin, Mao, Ma, Mengqi, Evans, Geoffrey M, 2022. Bed hydrodynamics of a new three-phase fluidized bed flotation column with steel ball particles. Miner. Eng. (ISSN: 0892-6875) 184, 107669. http://dx.doi.org/10.1016/j.mineng.2022.107669, URL https://www.sciencedirect.com/science/article/pii/S0892687522002795.

Hassanzadeh, Ahmad, 2018. A survey on troubleshooting of closed-circuit grinding system. Can. Metall. Q. (ISSN: 0008-4433) 57 (3), 328–340. http://dx.doi.org/10.1080/00084433.2018.1464618, Publisher: Taylor & Francis _eprint.

Hassanzadeh, Ahmad, Safari, Mehdi, Hoang, Duong H., Khoshdast, Hamid, Albijanic, Boris, Kowalczuk, Przemyslaw B., 2022. Technological assessments on recent developments in fine and coarse particle flotation systems. Miner. Eng. (ISSN: 0892-6875) 180, 107509. http://dx.doi.org/10.1016/j.mineng.2022.107509, URL https://www.sciencedirect.com/science/article/pii/S0892687522001194.

Herald, Matthew, Hampel, Dawid, Wheldon, Tzany Kokalova, Seville, Jonathan, Windows-Yule, Christopher, 2023. Monte Carlo model of the large modular array for positron emission particle tracking. IEEE Access (ISSN: 2169-3536) 11, 25982–25990. http://dx.doi.org/10.1109/ACCESS.2023.3255505, Conference Name: IEEE Access.

Islam, Md. Tariqul, Nguyen, Anh V., 2020. Parametric investigations of different variables on liquid–solid fluidization in a HydroFloat cell using computational fluid dynamics. Chem. Eng. Res. Des. (ISSN: 0263-8762) 159, 13–26. http://dx.doi.org/10.1016/j.cherd.2020.03.028, URL https://www.sciencedirect.com/science/article/pii/S0263876220301301.

Jameson, Graeme J., 2010. Advances in fine and coarse particle flotation. Can. Metall. Q. (ISSN: 0008-4433) 49 (4), 325–330. http://dx.doi.org/10.1179/cmq.2010.49.4.325, Publisher: Taylor & Francis _eprint.

Jameson, Graeme J., Cooper, Lonn, Tang, Kitty K., Emer, Cagri, 2020. Flotation of coarse coal particles in a fluidized bed: The effect of clusters. Miner. Eng. (ISSN: 0892-6875) 146, 106099. http://dx.doi.org/10.1016/j.mineng.2019.106099, URL https://www.sciencedirect.com/science/article/pii/S0892687519305102.

Jameson, Graeme J., Emer, Cagri, 2019. Coarse chalcopyrite recovery in a universal froth flotation machine. Miner. Eng. (ISSN: 0892-6875) 134, 118–133. http://dx.doi.org/10.1016/j.mineng.2019.01.024, URL https://www.sciencedirect.com/science/article/pii/S089268751930041X.

Janishar Anzoom, Sayed, Bournival, Ghislain, Ata, Seher, 2024. Coarse particle flotation: A review. Miner. Eng. (ISSN: 0892-6875) 206, 108499. http://dx.doi.org/10.1016/j.mineng.2023.108499, URL https://www.sciencedirect.com/science/article/pii/S0892687523005137.

Kohmuench, J.N., Luttrell, G.H., Mankosa, M.J., 2001. Coarse particle concentration using the HydroFloat separator. Min. Metall. Explor. (ISSN: 2524-3470) 18 (2), 61–67. http://dx.doi.org/10.1007/BF03402873.

Kromah, V., Powoe, S.B., Khosravi, R., Neisiani, Ali Asimi, Chelgani, S. Chehreh, 2022. Coarse particle separation by fluidized-bed flotation: A comprehensive review. Powder Technol. (ISSN: 0032-5910) 409, 117831. http://dx.doi.org/10.1016/j.powtec.2022.117831, URL https://www.sciencedirect.com/science/article/pii/S0032591022007161.

Mesa, Diego, Cole, Katie, van Heerden, Michael R., Brito-Parada, Pablo R., 2021. Hydrodynamic characterisation of flotation impeller designs using positron emission particle tracking (PEPT). Sep. Purif. Technol. (ISSN: 1383-5866) 276, 119316. http://dx.doi.org/10.1016/j.seppur.2021.119316, URL https://www.sciencedirect.com/science/article/pii/S138358662101025X.

Mesa, Diego, van Heerden, Michael, Cole, Katie, Neethling, Stephen J., Brito-Parada, Pablo R., 2022. Hydrodynamics in a three-phase flotation system – fluid following with a new hydrogel tracer for positron emission particle tracking (PEPT). Chem. Eng. Sci. (ISSN: 0009-2509) 260, 117842. http://dx.doi.org/10.1016/j.ces.2022.117842, URL https://www.sciencedirect.com/science/article/pii/S0009250922004262.

Nicuşan, A.L., Windows-Yule, C.R.K., 2020. Positron emission particle tracking using machine learning. Rev. Sci. Instrum. (ISSN: 0034-6748) 91 (1), 013329. http://dx.doi.org/10.1063/1.5129251, URL https://aip.scitation.org/doi/10.1063/1.5129251, Publisher: American Institute of Physics.

Parker, D.J., Broadbent, C.J., Fowles, P., Hawkesworth, M.R., McNeil, P., 1993. Positron emission particle tracking - a technique for studying flow within engineering equipment. Nucl. Instrum. Methods Phys. Res. A (ISSN: 01689002) 326 (3), 592–607. http://dx.doi.org/10.1016/0168-9002(93)90864-E, URL https://linkinghub.elsevier.com/retrieve/pii/016890029390864E.

Parker, David J., Hampel, Dawid M., Kokalova Wheldon, Tzanka, 2022. Performance evaluation of the current Birmingham PEPT cameras. Appl. Sci. (ISSN: 2076-3417) 12 (14), 6833. http://dx.doi.org/10.3390/app12146833, URL https://www.mdpi.com/2076-3417/12/14/6833, Number: 14 Publisher: Multidisciplinary Digital Publishing Institute.

Parker, D.J., Leadbeater, T.W., Fan, X., Hausard, M.N., Ingram, A., Yang, Z., 2008. Positron imaging techniques for process engineering: recent developments at Birmingham. Meas. Sci. Technol. 19 (9), 094004. http://dx.doi.org/10.1088/0957-0233/19/9/094004, (ISSN: 0957-0233, 1361-6501), URL https://iopscience.iop.org/article/10.1088/0957-0233/19/9/094004.

Parker, David, Wheldon, Carl, 2018. The Birmingham MC40 cyclotron facility. Nucl. Phys. News (ISSN: 1061-9127) 28 (4), 15–20. http://dx.doi.org/10.1080/10619127.2018.1463021, Publisher: Taylor & Francis _eprint.

Wang, Jianlong, Nguyen, Anh V., Farrokhpay, Saeed, 2016. A critical review of the growth, drainage and collapse of foams. Adv. Colloid Interface Sci. (ISSN: 0001-8686) 228, 55–70. http://dx.doi.org/10.1016/j.cis.2015.11.009, URL https://www.sciencedirect.com/science/article/pii/S0001868615002171.

Wiggins, Cody, Patel, Nitant, Bingham, Zachary, Ruggles, Arthur, 2019. Qualification of multiple-particle positron emission particle tracking (M-PEPT) technique for measurements in turbulent wall-bounded flow. Chem. Eng. Sci. (ISSN: 00092509) 204, 246–256. http://dx.doi.org/10.1016/j.ces.2019.04.030, URL https://linkinghub.elsevier.com/retrieve/pii/S0009250919303951.

Wills, Barry A., Finch, James A., 2016. Froth flotation. In: Wills' Mineral Processing Technology. Elsevier, ISBN: 978-0-08-097053-0, pp. 265–380. http://dx.doi.org/10.1016/B978-0-08-097053-0.00012-1, URL https://linkinghub.elsevier.com/retrieve/pii/B9780080970530000121.

Zanin, Massimiliano, Chan, Eddie, Skinner, William, 2021. Modelling the fluidised bed in HydroFloat™ for improved process control. Powder Technol. (ISSN: 0032-5910) 388, 241–250. http://dx.doi.org/10.1016/j.powtec.2021.04.089, URL https://www.sciencedirect.com/science/article/pii/S0032591021003764.